Geography and the Environment Faculty
Publications

Geography and the Environment

5-2018

Evaluation of Agricultural Land Cover Representations on Regional Climate Model Simulations in the Brazilian Cerrado

Stephanie A. Spera
University of Richmond, sspera@richmond.edu

Jonathan M. Winter

Jonathan W. Chipman

Follow this and additional works at: https://scholarship.richmond.edu/geography-faculty-publications

Part of the Agriculture Commons, and the Environmental Sciences Commons

Evaluation of Agricultural Land Cover Representations on Regional Climate Model Simulations in the Brazilian Cerrado

Stephanie A. Spera[1,2] iD, Jonathan M. Winter[2] iD, and Jonathan W. Chipman[2] iD

[1]Neukom Institute for Computational Science, Dartmouth College, Hanover, NH, USA, [2]Department of Geography, Dartmouth College, Hanover, NH, USA

Abstract Examining interactions between large-scale land cover and land use change and regional climate in areas undergoing dynamic land transformations, like the Brazilian Cerrado, is crucial for understanding tradeoffs between human needs and ecosystem services. Yet regional climate models often do not include accurate land cover data of these complex landscapes. We use National Center for Atmospheric Research's Weather Research and Forecasting (WRF) model coupled to the Noah-Multiparameterization (Noah-MP) land surface model to run 10-year climate simulations across Brazil to assess (1) whether an accurate, regionally validated land cover data set with two, new agricultural land cover classifications improves model simulation results; (2) the ability of Noah-MP's dynamic vegetation option to model vegetation growth; and (3) the sensitivity of the model output to scale. The results of the simulations with the updated land surface perform better over intensive agricultural areas for precipitation, evapotranspiration, and temperature, especially during the wet-to-dry season transition months. Evapotranspiration is overestimated during the start of the rainy season across all model simulations, which is likely due to the soil moisture model. We also find that using the Noah-MP dynamic vegetation significantly degrades agricultural leaf area index phenology simulations in Brazilian agricultural regions. Lastly, improving the model's resolution did not improve model output when compared to observational data. Incorporating more accurate representations of the landscape into regional climate models is essential for quantifying potential changes in climatological seasonality in dynamic, human-modified regions and making informed land use decisions.

Plain Language Summary Humans are the largest drive of landscape change globally. One region that exemplifies this change is Brazil's Cerrado—over half of it has been cleared for agriculture. Farmers in the region depend on a stable rainy season to cultivate crops like soy and corn, but, clearing Cerrado for agriculture may disturb regional climate and affect precipitation. The first step to assessing these impacts is determining whether a more accurate land surface improves simulation results and where the model still needs to be improved. We use the Weather Research and Forecasting (WRF) model to run 10-year-long climate simulations across Brazil with both the default U.S. Geological Survey land cover map and an updated land cover map with two new agricultural categories. Our results show that using an updated map improves model results over regions of intensive agriculture, especially in the dry-to-wet-season transition months. All simulation results show an overestimation in evapotranspiration rates and a cold bias during the rainy season. These biases seem to be the result of WRF's soil-moisture model. Understanding both these interactions and how we can use climate models to better study them is essential for making informed land use decisions.

1. Introduction

Understanding interactions between large-scale land cover and land use change and regional climate in food exporting countries is essential to creating effective policies that incentivize sustainable agricultural practices, especially when considering issues such as population growth, food security, and climate change. In new, dynamic, global breadbaskets like Brazil, where over 20% of the country's gross domestic product is dependent on the agribusiness sector (Vendemiatti & Berk, 2016), and agricultural commodities are exported worldwide, the stakes are even higher. Brazil is the top producer and exporter of sugar, coffee, and orange juice; leads the world in chicken and soy production and is second only to the United States in exports; and is second in beef production only to India (Simoes & Hidalgo, 2011).

Here we focus our efforts on the Brazilian Cerrado, the 2 million km^2 savannah biome in which more than half of Brazil's agriculture is cultivated. The region, a biodiversity hot spot, is characterized by distinct wet and dry seasons: nearly 90% of the average 1,500 mm of annual precipitation falls during the wet season, which spans October to April (Klink & Machado, 2005). To date, over half of the biome has been cleared and massive land cover changes continue to occur, primarily in the form of conversion of natural vegetation and pasture to export-oriented agriculture like soy. However, because less than 2% of Brazil's agriculture is irrigated (The World Bank, 2017), land use-climate feedback may affect the regional water and energy balances and upend the successful production of large-scale export-oriented agriculture in the region (Coe et al., 2017; Oliveira et al., 2013).

Land use changes in Brazil affect the water and energy balance through changes in albedo, surface rough-ness, and latent and sensible heat fluxes. Precipitation in the Amazon and the Amazon-Cerrado transition region is dependent on evapotranspiration (ET; Lee et al., 2012; Wright et al., 2017), and the deep roots of the natural vegetation of the Amazon and Cerrado allow for continued deep water access and transpiration throughout the dry season (Nepstad et al., 1994). Furthermore, land use changes in the Amazon and Cerrado have resulted in heavily fragmented landscapes (Arima et al., 2016). The atmospheric boundary layer above a humid forest is less stable than that above a deforested area (Wang et al., 2009). Mesoscale circulations and greater sensible:latent heat ratio caused by heterogeneous deforested surfaces create a lifting mechanism that supports shallow convection over deforested areas (Wang et al., 2009). Intact forested areas, however, both generate more convective available potential energy, and lack that lifting mechanism, which results in deep cloud formation over forested regions as compared to shallow cloud formation over deforested areas (Wang et al., 2009). Thus, the conversion of natural forest to pasture and row-crop agriculture have noticeably affected the regional water and energy balance across the Brazilian Amazon and Cerrado through observed decreases in precipitation (Butt et al., 2011; Dubreuil et al., 2012; Fu et al., 2013) and evaporation (Lathuillière et al., 2012; Oliveira et al., 2014; Spera et al., 2016) and increases in fire occurrence (Aragão et al., 2008), streamflow (Costa et al., 2003; Hayhoe et al., 2011; Panday et al., 2015), and temperature (Dubreuil et al., 2012; Panday et al., 2015; Silvério et al., 2015).

Climate modeling studies demonstrate both that native vegetation and the land cover replacing that cleared vegetation play an important role in regulating regional climate. For example, Bagley et al. (2014) found that deforestation in the Amazon could exacerbate drought conditions (Bagley et al., 2014); Costa and Pires (2010) showed that a simultaneous deforestation of the Amazon and total deforestation of the Cerrado increase the length of the dry season from five to six months, and Malhado et al. (2010) and Coe et al. (2017) demonstrated that the Cerrado itself plays a crucial role in maintaining rainfall over the Amazon. And, the land cover replacing these cleared areas matters. A modeling experiment demonstrated that the complete expansion of soybean onto deforested lands in the Amazon led to greater decreases in precipitation than if that land were cultivated with pasture grasses (Costa et al., 2007). In the Cerrado, Loarie et al. (2011) concluded that sugarcane transfers water and energy more similarly to the Cerrado's natural vegetation than pasture or soybean.

An accurate land cover data set is a crucial component of any climate modeling experiment. However, vege-tation parameters—such as leaf area index (LAI), vegetation fraction (FVEG), and stomatal resistance (see Table S3 for complete list of those set in Weather Research and Forecasting, WRF)—are typically set to fixed values from tables that are not specific to the region or regional flora. This simplification inhibits the ability to understand both land-atmosphere interactions and projections of land-atmosphere interactions under historical and future climates. Furthermore, existing land use and land cover data sets —such as the U.S. Geological Survey (USGS) Global Land Cover Characterization data set, which is based on Advanced Very High Resolution Radiation (AVHRR) data from 1992 and 1993, or the 2001 Moderate Resolution Imaging Spectroradiometer (MODIS) International Geosphere-Biosphere Programme Land Cover data—do not cap-ture the dynamics and complexity of heavily modified landscapes like that of the Brazilian Cerrado. Finally, as described above, many land cover-change-climate modeling studies of the region focus on the complete conversion of one land cover type to another rather than dynamic transitions among land cover types.

Here we use the Advanced Research WRF model to run continuous decade-long simulations to assess (1) whether a highly accurate, regionally validated land cover data set improves model simulation result; (2) the ability of WRF running the Noah-Multiparameterization land surface model with dynamic vegetation to
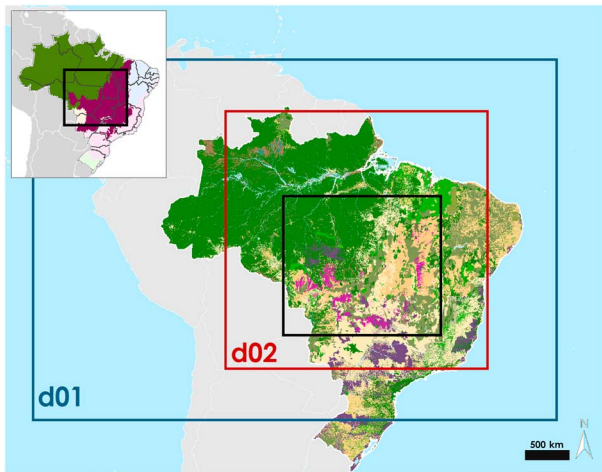
Figure 1. WRF domains and Brazil's updated land cover map. The black box indicates our specific area of interest. The land cover basemap is a merger of the 2002 PROBIO data set (Sano et al., 2010) and Spera et al. (2016) 2008 growing season large-scale agriculture map. Forested areas are green; Cerrado, pasture, and grasslands are yellow and tan; PROBIO's agropastoral lands are purple; and the Spera et al. (2016) row-crop agriculture is pink. Inset. Brazil and its six biomes are highlighted, the Amazon biome is dark green, and the Cerrado biome is magenta.

accurately model vegetation growth; and (3) the sensitivity of the model output to domain resolution. Importantly, this study leverages a novel land cover data set (Spera et al., 2016) that includes two agricultural rotations common across Brazil today: soy single cropping and soy-corn double cropping. Incorporating these land covers into regional climate model simulations is the first step to being able to provide insights into realistic land cover-regional-climate feedback and improve future agricultural planning and management decisions.

2. Methods

2.1. Model Setup

We used the Advanced Research WRF model v3.8.1 (Skamarock et al., 2008), maintained by the National Center for Atmospheric Research, coupled to the Noah-Multiparameterization (Noah-MP) land surface model (Niu et al., 2011; Yang et al., 2011). Our model domain includes the entirety of the Cerrado and Brazilian Amazon (d01, Figure 1). To assess the sensitivity of the model to the land cover characterization and the performance of the dynamic vegetation model, we configured the model using a single domain at 36 km grid spacing (178 by 122 grid points) with a 120 s time step and daily output. We also used a two-way nested inner 12 km domain (d02, Figure 1) to determine the effects of scale/model resolution on performance. Six-hourly European Centre for Medium-Range Weather Forecasts Reanalysis-Interim (ERA-I) surface and pressure level data (Dee et al., 2011) provided the lateral boundary conditions.

To determine which set of parameterization schemes best simulated regional climate over Brazil, we tested eight possible combinations commonly cited in the literature (Table S1). Our final simulations used the Rapid Radiative Transfer Model (RRTM) to simulate shortwave and longwave radiation, WRF single-moment 6-class (WSM6) scheme to simulate microphysics, the Grell 3D scheme for the cumulus parameterization, the revised MM5 scheme for the surface layer, and the Yonsei University (YSU) scheme for the planetary boundary layer.

Six 10-year (2004–2013) simulations were conducted (Table 1). We allowed the model to spin up from January 2004 to July 2005 and focus our analysis on the nine growing seasons that occur in our study period beginning with the 2005 harvest year (August 2004 to July 2005) and ending with the 2013 harvest year.

We used the Noah-MP land surface model in WRF because it provides the user with multiple options to simulate land surface interactions (Niu et al., 2011). Specifically, Noah-MP integrates prescribed data and dynamic modeling to simulate the surface. This flexibility has the advantage of constraining model simulations over historical time periods for which vegetation input data are available, as well as allowing for dynamic vegetation, where the vegetation responds climate projections and is thus not constrained by historical vegetation parameters. The Noah-MP dynamic vegetation representation incorporates a photosynthesis-based stomatal resistance model and allows the user to define vegetation parameters completely or partly based on look-up

Table 1
Suite of Initial Simulations

Simulation	Land cover	Dynamic vegetation option	Simulation duration	Nested domains	Output frequency
1: USGS_DVoff	USGS	LAI table, FVEG prescribed	January 2004 to January 2014	No	Daily
2: USGS_DVfveg	USGS	LAI table, FVEG calculated	January 2004 to January 2014	No	Daily
3: USGS_DVall	USGS	LAI predicted, FVEG calculated	January 2004 to January 2014	No	Daily
4: USGS_nest	USGS	LAI table, FVEG prescribed	January 2007 to September 2008	Yes	Daily
5: IALU_DVoff	Spera et al. (2016)	LAI table, FVEG prescribed	January 2004 to January 2014	No	Daily
6: IALU_DVfveg	Spera et al. (2016)	LAI table, FVEG calculated	January 2004 to January 2014	No	Daily
7: IALU_DVall	Spera et al. (2016)	LAI predicted, FVEG calculated	January 2004 to January 2014	No	Daily
8: IALU_nest	Spera et al. (2016)	LAI table, FVEG prescribed	January 2007 to September 2008	Yes	Daily
9: IALU_3hr	Spera et al. (2016)	LAI table, FVEG calculated	January 2004 to January 2014	No	3-hourly

tables. When turned completely on, the dynamic vegetation model simulates both LAI and FVEG based on process-based equations and parameters from fixed land cover categories. The options chosen for our suite of simulations are provided in Table 1. We employed the Ball-Berry canopy resistance scheme simulations where we use the dynamic vegetation model to predict LAI and FVEG.

The user can choose from five different vegetation options, which control how the model treats LAI and FVEG. The four dynamic vegetation options tested were as follows: (1) dynamic vegetation turned off and both LAI and FVEG are prescribed; (2) FVEG is calculated from a table of monthly LAIs using equation (1); SAI is a land category's monthly stem area index; (3) the dynamic vegetation model turned thus using WRF's carbon allocation model to predict LAI and FVEG is set to the maximum vegetation fraction; and (4) dynamic vegetation turned on with LAI predicted from the carbon allocation model, and FVEG is calculated based on equation (1). Results from both simulations where the "dynamic vegetation" option is turned on and LAI is predicted were similar; thus, we only discuss the results of runs where dynamic vegetation is turned on completely in the main text. We did not test the fifth vegetation option in Noah-MP, where dynamic vegetation is turned off, monthly LAI is read from a look-up table, and FVEG is set to a static look-up table value because this option was not recommended for use by WRF.

$$FVEG = 1 - e^{(-0.52*(LAI+SAI))} \qquad (1)$$

2.2. Land Cover Data Sets

The WRF model provides two land use and land cover data sets: a 24-category USGS data set and a 21-category MODIS-based data set, to represent the land surface. The 1 km resolution USGS data set, the Global Land Cover Characterization, is based on an unsupervised classification of Advanced Very High Resolution Radiometer (AVHRR) vegetation index data collected between April 1992 and March 1993. The MODIS Land Cover Type Product (Friedl et al., 2002, 2010) is the result of a supervised classification that relies on MODIS Land Surface Temperature and Bidirectional Reflection Distribution Function data products. Although the USGS data set is older, we chose to use the USGS data set for comparison because it more accurately represented Brazilian land cover as classified by Sano et al. (2010) (see Figures S1 and S2). The default USGS land cover map does not differentiate between row-crop agriculture LAI and pastureland LAI. The two land cover categories, "dryland cropland and pasture" and "mixed dryland/irrigated cropland and pasture," have the same monthly LAIs in the Noah-MP vegetation look-up table.

We created an improved land cover data set inclusive of agricultural land use, hereafter IALU (Figure 1), by overlaying the mode land classification from the Spera et al. (2016) MODIS-based 250-m 2002–2016 agricultural data set onto the Landsat-based PROBIO Brazilian land cover classification (Sano et al., 2010). The PROBIO land classifications were mapped to the appropriate USGS land categories (Table S3), with two major exceptions. We converted the USGS "dryland crop and pasture" category to a single-cropping soy rotation, and the "irrigated crop and pasture" category to a soy-corn double-cropping rotation, because Brazil currently has limited irrigated agriculture. We also adjusted the monthly average leaf area indices of these two land classes according to MODIS LAI data product (MCD15A2H) of these land covers as mapped in Spera et al. (2016; Table S4).

Our full WRF model domain contained 21,716 grid cells. Our region of interest (black box, Figure 1) contained 2,296 grid cells. Of those grid cells, 61 were categorized as a single-cropping rotation and 149 were characterized by a double-cropping rotation after the IALU land cover was scaled up to a 36 km resolution. Because average annual rainfall varies between 400 and 2,600 mm/year across our study area, we subset our area into four different regions: the Mato Grosso Amazon-Cerrado transition, southwestern Mato Grosso and southern Goiás, Tocantins, and western Bahia, southern Maranhão, and southern Piauí (Figure S3). However, because results did not vary widely across the different regions, for the sake of brevity and readability, a majority of the results we present and discuss in the main text have been spatially averaged across our entire region of interest. All other results are provided in the supporting information.

2.3. Observational Data

Modeled precipitation, and minimum, maximum, and mean temperature were compared to Climate Research Unit (CRU) v 3.24.01 0.5° gridded precipitation and temperature data (Harris et al., 2014).

Modeled ET was compared to MODIS (MOD16A2) monthly 1 km ET data (Mu et al., 2007, 2011). The MODIS ET data are derived from National Aeronautics and Space Administration's Global Modeling and Assimilation Office daily meteorological reanalysis data, and MODIS albedo, LAI, the fraction of absorbed photosynthetically active radiation, and land cover data sets (Mu et al., 2011), and is an estimate of total plant transpiration, wet canopy evaporation, and soil evaporation based on the Penman-Monteith equation (Mu et al., 2011).

The MODIS and CRU data we compare our modeled results to are not without error. The MODIS ET product is a derived product based on both static and updated data. Ruhoff et al. (2013) note that eight-day MODIS ET data often underestimate ET and cite the MODIS land cover input as the largest source of error in the product's creation. However, they also show that when these data are aggregated to the monthly time scale, the data show good agreement with observations (Ruhoff et al., 2013). Loarie et al. (2011) compare the eight-day MODIS ET product to measurements from 10 eddy flux tower cites across Brazil over different land covers. They find that over the Cerrado, the mean bias is −0.04 mm/day, the root-mean-square error (RMSE) is 0.55 mm/day, and the annual bias is less than 4% (Loarie et al., 2011).

Gridded CRU temperature and precipitation data are based on interpolated monthly data collected at 4,800 stations around the world. Although CRU data have been previously used as the observed data set of comparison in regional climate studies over Brazil (Da Rocha et al., 2015; Lee & Berbery, 2012), because there exists poor station data coverage in the interior of South America our "observed" data set may be biased and underestimate spatial and interannual variability (Malhi & Wright, 2004; New et al., 1999). In an analysis comparing various gridded precipitation data sets, including CRU, to Agencia Nacional de Aguas streamflow data, Levy et al. (2017) demonstrated that over the Brazilian rainforest-savanna transition zone, which overlaps with our study region, the Precipitation Estimate from Remotely Sensed Information using Artificial Neural Networks (PERSIANN) data set is the best observational data set for the region. In comparing the CRU data set to the PERSIANN data set, we find that the CRU data set closely aligns with the PERSIANN data set in Bahia, Piauí, Maranhão region, and Goiás and southwestern Mato Grosso (Figure S4). During the height of the rainy season, CRU monthly precipitation is slightly underestimated as compared to PERSIANN across Tocantins and the Mato Grosso Amazon-Cerrado transition zone, but the seasonal cycle is still intact (Figure S4). These results are expected, as there are likely more temperature and precipitation stations closer to Brazil's coast, and fewer within the country's interior. Thus, we note that CRU data may underestimate average precipitation across our region and address this in the results and discussion.

2.4. Model Performance

To assess model performance at both model spatial resolutions, we calculated the total error (RMSE), systematic error (bias), and nonsystematic errors (RMSEdb) according to Ruiz et al. (2010) and Pei et al. (2014) within our area of interest (black box in Figure 1) for each month in the year.

$$\text{RMSE} = \sqrt{\frac{\sum (m_i - o_i)^2}{N}} \tag{2}$$

$$\text{bias} = \frac{\sum (m_i - o_i)}{N} \tag{3}$$

$$\text{RMSEdb} = \sqrt{\frac{\sum (m_i - o_i - \text{bias})^2}{N}} \tag{4}$$

We also derived 95% bootstrap confidence intervals around the mean for each output variable of interest for each month of both observed data and modeled data to assess which simulations best model the seasonal cycle of the aforementioned variables. We focused on just those grid cells that are predominantly in a single-cropping or double-cropping rotation as classified by the IALU land cover data set. We used bootstrapping (1,000 resamples) to estimate these confidence intervals because no assumptions of the underlying data distributions are required. We then compared the modeled data to the observed data to determine whether the modeled observations overlap with the 95% confidence intervals of the observed data (Challinor et al., 2014; Legates & McCabe, 1999).

Table 2
Table of Secondary Simulation Run to Determine Sources of Model Error

Simulation	Simulation duration	Cumulus scheme	Soil moisture factor for stomatal resistance	Surface evaporation resistance option	Stomatal resistance	Max and field soil moisture content
IALU_C (original configuration)	January 2004 to January 2010	Grell 3D	Default Noah	Default Sakaguchi and Zeng (2009)	Default table values	Default table values
IALU_ A	January 2004 to January 2010	Kain-Fritsch	Default Noah	Default Sakaguchi and Zeng (2009)	Default table values	Default table values
IALU_ btr2	January 2004 to January 2010	Grell 3D	CLM	Default Sakaguchi and Zeng (2009)	Default table values	Default table values
IALU_ btr3	January 2004 to January 2010	Grell 3D	SSiB	Default Sakaguchi and Zeng (2009)	Default table values	Default table values
IALU_ rsf2	January 2004 to January 2010	Grell 3D	Default Noah	Sellers et al. (1992)	Default table values	Default table values
IALU_ rsf3	January 2004 to January 2010	Grell 3D	Default Noah	Adjusted Sellers et al. (1992) to account for wet soil	Default table values	Default table values
IALU_ rsX4	January 2004 to January 2010	Grell 3D	Default Noah	Default Sakaguchi and Zeng (2009)	Agricultural land cover values quadrupled	Default table values
IALU_smc	January 2004 to January 2010	Grell 3D	Default Noah	Default Sakaguchi and Zeng (2009)	Default table values	SMC values halved

We are especially interested in the model's performance during the dry-to-wet season transition, as a long, stable rainy season is crucial for double cropping (Spangler et al., 2017); recent work has demonstrated the importance of regional dry-season transpiration on the creation of a shallow convection moisture pump and thus the start of the rainy season (Wright et al., 2017), and the biggest differences in ET rates between land covers occur during the transition and dry seasons (Georgescu et al., 2013; Oliveira et al., 2014; Spera et al., 2016).

As presented and discussed below, all model simulations both overestimated ET during the start of the rainy season across all model simulations and exhibited a cold bias during the rainy season. Thus, we performed additional five-year long model runs with daily and three-hourly output using the IALU land cover, LAI table, and prescribed FVEG prescribed to attempt to determine the sources of these errors within the model. We tested the sensitivity of the model temperature output by using the Kain-Fritsch cumulus scheme (Table 2: IALU_A); we tested the sensitivity of the model ET output by changing the surface evaporation resistance option (Table 2: IALU_rsf2 and IALU_rsf2), the soil moisture factor for stomatal resistance (Table 2: IALU_btr2 and IALU_btr3), quadrupling the baseline stomatal resistance of the agricultural land cover categories (Table 2: IALUS_rsX4), and halving the maximum and reference soil moisture content parameters of the soils present in our study region (Table 2: IALU_smc).
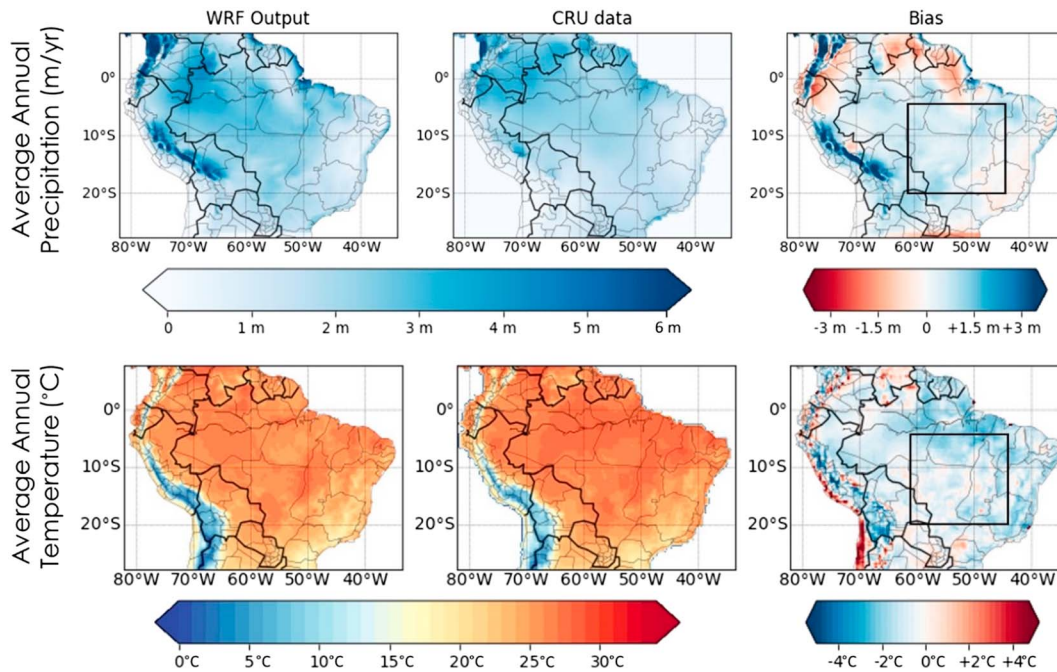
3. Results and Discussion

3.1. Regional Evaluation of WRF

As shown in Table 3 and Figure 2 (black box), all the simulations perform reasonably well over our region of interest. Across the entire simulation domain, the largest biases in both temperature and precipitation occur along the Andes, which are outside of our area of interest and not surprising given the complex coastline and dramatic topography. All simulations demonstrate a wet bias across much of our study area, similar to other studies using WRF in the same region of interest (Georgescu et al., 2013). However, this slight wet-bias may also be an artifact of CRU's underestimation of precipitation during the rainy season (Figure S4). Simulations with the dynamic vegetation turned completely on have lower annual precipitation RMSEs than other runs, but large annual temperature and annual ET RMSEs and ET biases.

Table 3
Total Error (RMSE), Systematic Error (Bias), and Nonsystematic Errors (RMSEdb) of All Simulations

| Precipitation (mm/year) Annual average: 1,694 mm/year	RMSE	Bias	RMSEdb
IALU_ DVoff	80.66	33.60	68.49
USGS_DVoff	80.50	33.69	68.72
IALU_DVfveg	81.75	35.22	68.79
USGS_DVfveg	78.37	32.17	66.83
IALU_DVon	78.13	31.23	65.74
USGS_DVon	76.66	30.67	64.43
Mean temperature (°C/year) Annual average: 26.1 °C	RMSE	Bias	RMSEdb
IALU_ DVoff	1.55	−0.93	1.07
USGS_DVoff	1.53	−0.81	1.10
IALU_DVfveg	1.60	−0.90	1.10
USGS_DVfveg	1.64	−0.81	1.17
IALU_DVon	1.98	−1.52	1.09
USGS_DVon	1.97	−1.57	1.03
Evapotranspiration (mm/year) Annual average: 1,123.92 mm/year	RMSE	Bias	RMSEdb
IALU_ DVoff	183.93	2.61	182.01
USGS_DVoff	184.30	2.65	182.21
IALU_DVfveg	183.85	1.72	181.96
USGS_DVfveg	184.17	1.13	182.22
IALU_DVon	183.16	6.89	181.97
USGS_DVon	183.08	7.18	181.96

Figure 2. (top) Average annual precipitation in m/year and (bottom) temperature in °C across our model domain from the WRF simulation. IALU_DVfveg output is shown in the first column panels, and observed CRU data are displayed in the second panels. Biases (WRF-CRU) are shown in the third column. Our region of interest is outlined in black in the third column.

3.2. Dynamic Vegetation Model

The USGS agropastoral categories (pink lines, Figure 3) are characterized by one large annual increase in leaf area that both preempts and overestimates the observed increase in leaf area. The LAIs of the IALU modified single-cropping and double-cropping categories (blue lines, Figure 3) were based on MODIS LAI phenology. The IALU modeled LAIs closely match the average observed MODIS LAIs of single- and double-cropped regions in our study area (green lines, Figure 3). The model runs where Noah-MPs dynamic vegetation driver predict LAI (dotted lines, Figure 3) simulate the LAI phenology over the growing season poorly.

3.3. Sensitivity of WRF to Land Use Over the Cerrado

The IALU model runs perform similarly to USGS model runs over single-cropped areas (Figures 4a, 4c, and 4e and Tables S5–S9) but outperform the USGS model runs over double cropped areas (Figures 4b, 4d, and 4f and Tables S5–S9). As shown in Figures 4b, 4d, and 4f, the bootstrapped 95% ET, precipitation, and
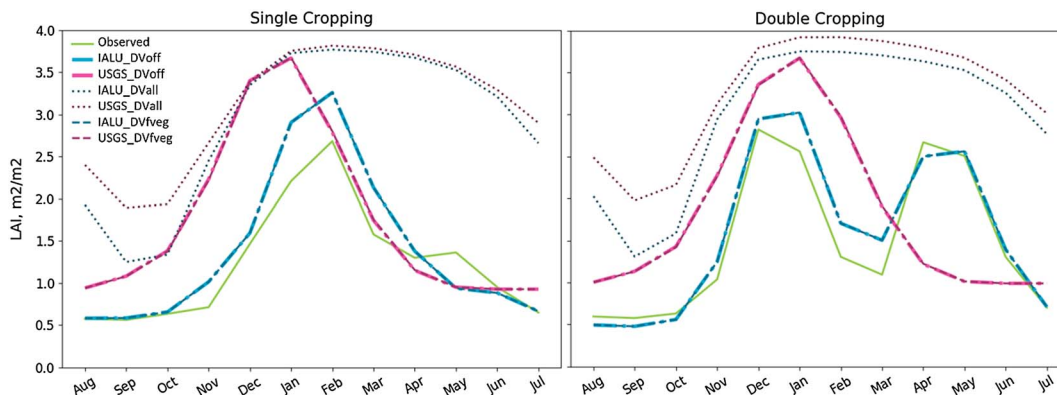
Figure 3. Observed MODIS LAIs (green) of grid cells characterized by (right) single-cropped land cover and (left) double-cropped land cover. Monthly LAI of the default WRF USGS table and dynamic vegetation model output are in magenta, and the modified LAI of the IALU land surface is in blue.
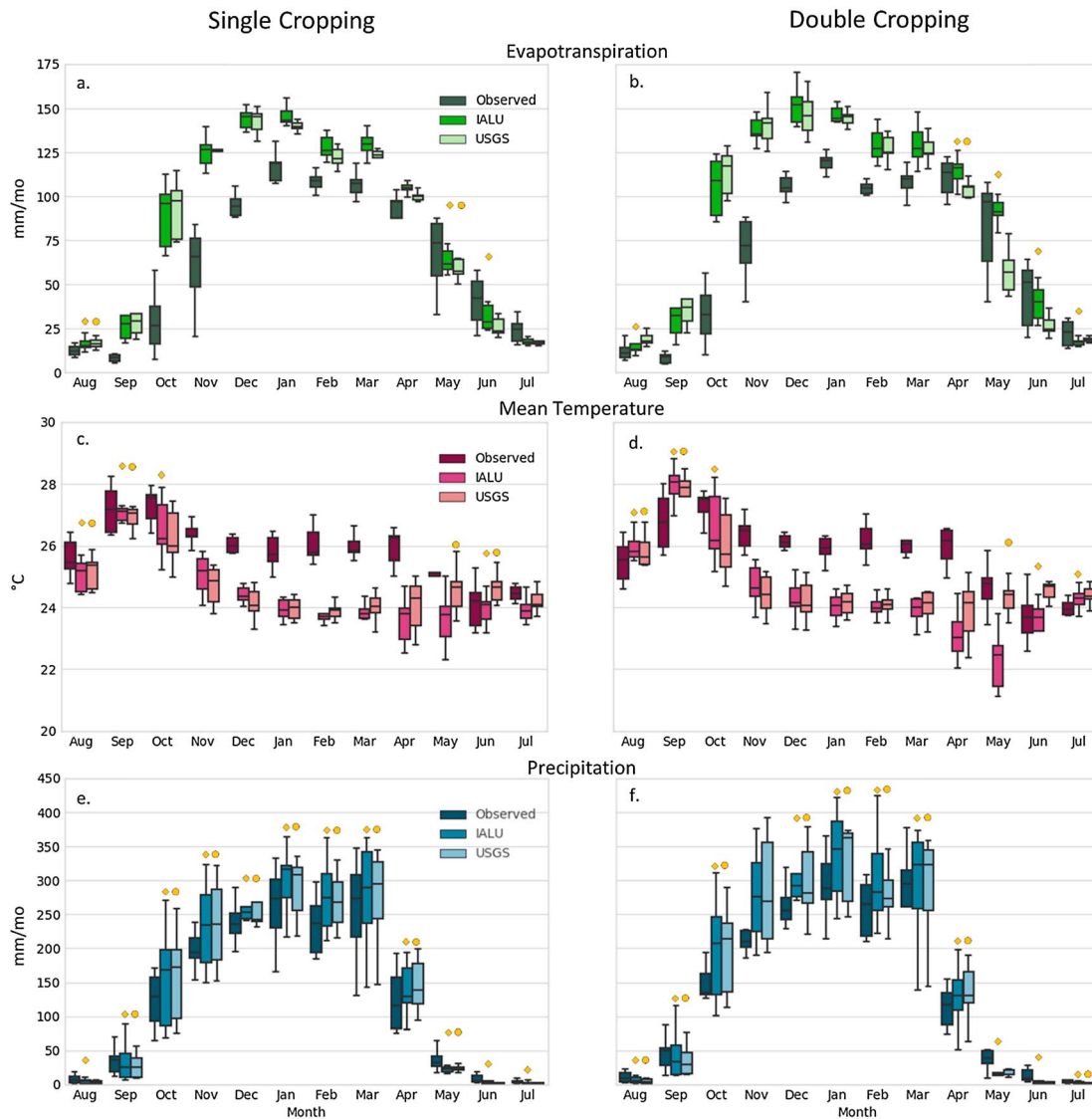
Figure 4. (a and b) Box plots of the observed (MODIS) evapotranspiration (dark green), (c and d) (CRU) temperature (dark red), and (e and f) (CRU) precipitation (dark blue) and WRF modeled temperature, precipitation, and evapotranspiration over the growing season in grid-cells characterized by (a, c, and e) and double-cropping rotations (b, d, and f) in the IALU land cover. Note that these results are the spatial average across our study area of interest (black box, Figure 1). Shown here are the results for IALU_DVfveg (green, pink, blue) and USGS_DVfveg (light green, light pink, and light blue). The yellow diamonds signify months where the bootstrapped 95% confidence intervals of observed and modeled IALU results overlap. The yellow circles signify months where the bootstrapped 95% confidence intervals of observed and modeled USGS results overlap. Results for USGS_DVoff, IALU_DVoff, USGS_DVall, and IALU_DVall are included in the supporting information.

temperature confidence intervals of the IALU model runs overlap with those of the observed data in more months than the USGS land cover model runs, yet all simulations struggle to accurately reproduce wet season climate across all variables. The IALU model simulations especially perform better compared to those with the USGS land covers during the dry season and the dry-to-wet-season transition (May—August) for those grid cells characterized by double-cropping rotations. Of the six model simulations, those with the dynamic vegetation turned completely on (USGS_DVall and IALU_DVall) perform the most poorly at accurately capturing the climatic seasonal cycles (Tables S5–S9).

The DVoff model runs perform comparably to their paired DVfveg simulations (Tables S5–S9). As Pei et al. (2014) highlight, the WRF model is extremely sensitive to the land surface processes. Because DVoff and DVfveg model runs both rely on the LAI look-up table, and LAI strongly controls FVEG which, in turn, controls surface processes including the portioning of the surface energy budget, ET, and temperature, it follows then that these model runs would have similar output.
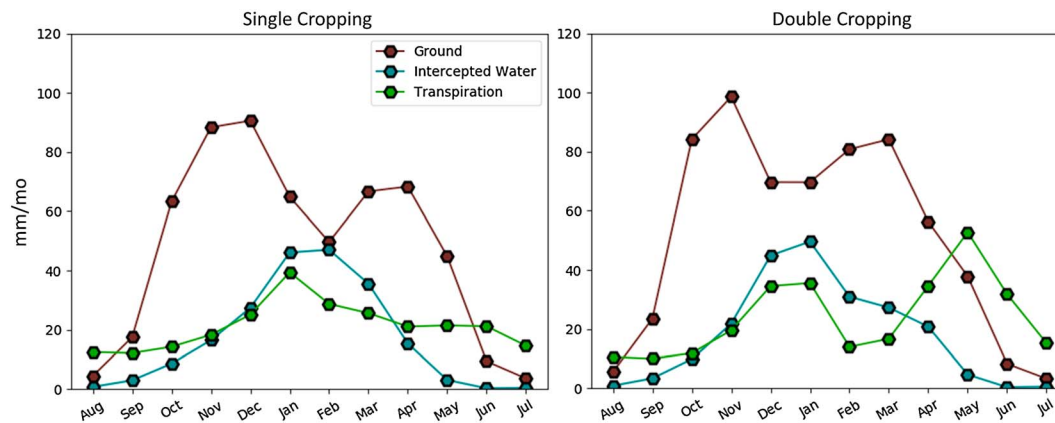
Figure 5. Average monthly evapotranspiration output of IALU_3hr run broken down into soil evaporation (brown), intercepted water evaporation (blue), and transpiration (green).

3.4. Evapotranspiration

The four IALU model simulations have more monthly overlapping confidence intervals than the default USGS land covers over areas that are double-cropped, especially during the dry season and wet-dry season transitions (Figures 4a and 4b and Table S5). Aside from the IALU_DVall simulation output in April and May for double-cropping grid cells, no other monthly confidence intervals overlap for either DVall simulation for either cropping rotation (Table S5).

All models overestimate ET during the early part of the rainy season, sometimes twofold or threefold in September, October, and November (Figures 4a and 4b). Furthermore, unlike the temperature and precipitation biases, this overestimation in ET does not occur homogenously across the domain. ET is overestimated fourfold during these months in both Mato Grosso and Goiás yet only, at most, twofold during these months across the drier Matopiba region (Figure S5). Modeled ET is overestimated across two thirds of the year in Goiás and southwestern Mato Grosso (Figure S5).

As described in detail below, the overestimation of ET during the early part of the rainy season is likely a result of excessive evaporation from Noah-MP's soil moisture model. As shown in Figure 5, soil evaporation comprises over 75% of the total ET output in these months. Year-long WRF/Noah-MP simulations over the Southern Great Plains also resulted in an overestimation of summer ET, which was directly caused by a wet top-soil-moisture layer (Pei et al., 2014). We describe the results of determining the physical mechanisms behind this overestimation in section 3.8 below.

3.5. Temperature

All models simulate the increase and fall in average temperature at the beginning of the rainy season (Figures 4c and 4d and Table S6). However, all models then severely underestimate temperature for the next seven to eight months (Figures 4c and 4d and Table S6). Again, the DVall models perform worst at simulating temperature, with only the September and October confidence intervals of IALU_DVall overlapping with those of the CRU data for single- and double-cropped grid cells, and only the October confidence interval of USGS_DVall overlapping for both cropping rotations (Table S6).

We further explored these biases in average surface temperature by analyzing the simulated and observed seasonal cycles of maximum and minimum surface temperature (Tables S7 and S8). The models perform better at simulating minimum temperature than maximum temperature (Tables S7 and S8). Monthly confidence intervals of minimum temperature overlap with observed data in 10 months of the year over single-cropped grid cells for all simulations except USGS_DVall and IALU_DVall, which had five and three months overlap, respectively. Of the double-cropping grid-cells, the IALU simulations have more months overlap than the corresponding USGS simulation, with the DVfveg simulations performing worse (Table S7). When the confidence intervals of the modeled data do not overlap, the model typically overestimates minimum temperature by about 1 °C.

The model's ability to reconstruct maximum temperature, then, plays a large role in the cold bias. All of the models underestimate rainy season (October–April) maximum temperature by 1–3 °C (Table S8). USGS_DVoff
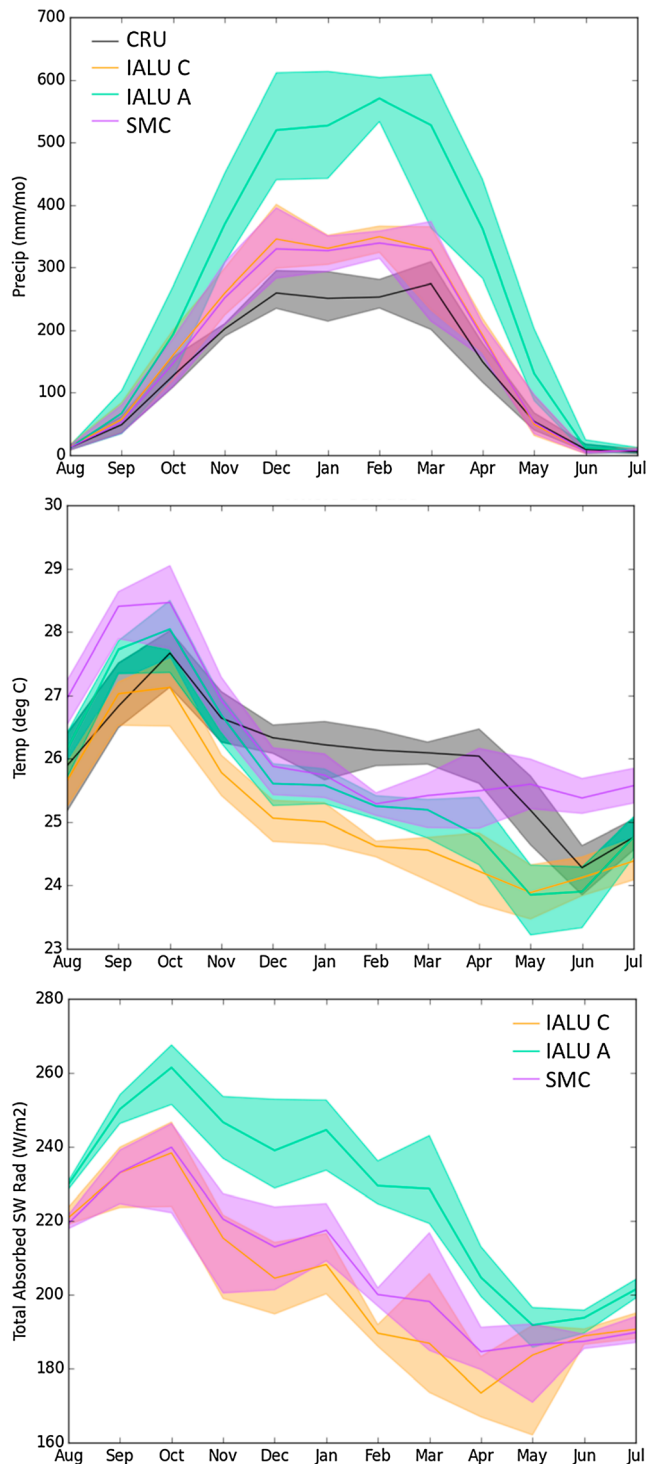
Figure 6. Comparison of observed (CRU black) data to modeled data (orange, teal, and purple) for (top) average monthly precipitation, (middle) temperature, and (bottom) absorbed shortwave radiation. The solid lines represent mean monthly values, while the shaded area represents bootstrapped 95% confidence intervals. Results for subregions are presented in the supporting information.

performed best at simulating maximum temperature correctly in four months (May, June, August, and September) over singled-cropped grid cells and five months (May–September) over double-cropped grid cells (Table S8).

These temperature biases may be caused by the cumulus scheme, soil moisture scheme and adjusted vegetation parameters, the ERA-Interim data used for all simulations' boundary conditions, or some combination these variables. Much of the work with WRF in South America is on short-term weather forecasting, and few studies use Noah-MP or discuss climatological temperature biases for longer-term simulations. Ruiz et al. (2010) evaluated WRF model sensitivity to different parameterization schemes for 48-hr forecasts over South America and found that surface temperature was sensitive to both cumulus scheme and surface processes, but the Grell cumulus scheme simulation exhibited a cold bias that increased over time. This cool bias is particularly evident during the October–March rainy season, when there are clouds overhead. Moreover, Massey et al. (2016) demonstrated that an overestimation of soil moisture was the primary source of cold biases over the United States' Great Plains. Year-long simulations over the Southern Great Plains that use both Noah-MP and a Grell-3D cumulus scheme, as in these simulations, also result in a three-degree cold bias (Pei et al., 2014). The Noah-MP LSM is extremely sensitive to surface dryness factor, saturated hydraulic conductivity, and saturated soil moisture, yet these variables are both often highly uncertain for different soil types and regions, with arid and semiarid regions being particularly problematic (Cai et al., 2014; Pei et al., 2014). ERA-Interim data, which was used for all simulations' boundary conditions, has been shown to exhibit inherent bias (Gao et al., 2014; Ruiz-Arias et al., 2016). However, the ERA-Interim data exhibit a warm bias over our study area (Figure S6). Thus, it is likely that the cold bias across our results is related to both ET dynamics within the Noah-MP land surface model and the chosen surface layer and cumulus schemes, and we describe these results of testing in section 3.8.

3.6. Precipitation

IALU_DVfveg precipitation matches observations for all months over single-cropped grid cells (Figure 4e) and 11 months over double-cropped grid cells (Figure 4f): November precipitation is overestimated. USGS_DVfveg precipitation matches observations over single-cropped areas in 11 months: July precipitation is underestimated (Figure 4e), and matches observations in double-cropped areas for just nine months: overestimating precipitation in November, and underestimating May and June precipitation (Figure 4f). All models capture the seasonal cycle in precipitation reasonably well. IALU_DVoff precipitation matches that of observed precipitation for all months and over single-cropped and double-cropped grid cells (Table S9). USGS_DVoff precipitation matches observations over single-cropped and double-cropped areas for 11 months: July precipitation is underestimated (Table S9). IALU_ and USGS_DVall precipitation confidence intervals overlap with observed for the entire year for single-cropped areas and 11 months for double-cropped areas: May precipitation is underestimated (Table S9).

3.7. Scale

We hypothesized that a second, higher-resolution (12 km) nested domain might improve results by capturing smaller-scale processes because the land cover data set would be used at a higher resolution. However, the
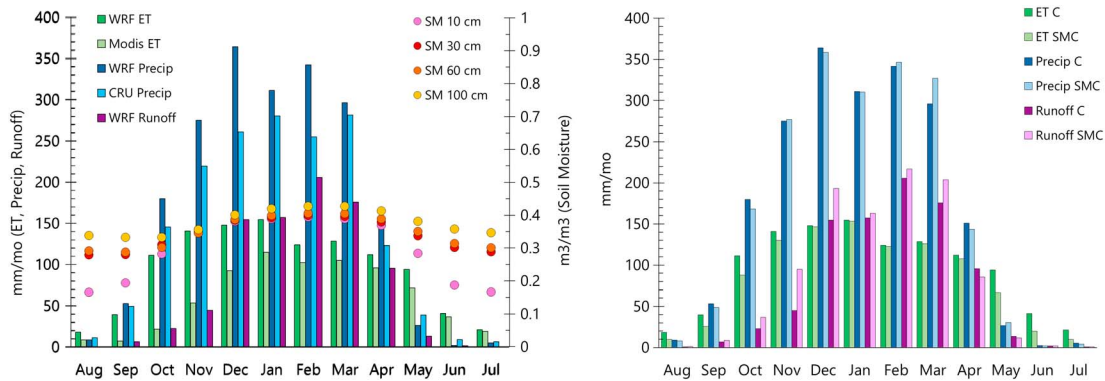
Figure 7. (left) Average monthly evapotranspiration (green), precipitation (blue), and runoff (purple) of model results (IALU_C, double cropping across whole study area) and observed CRU and MODIS data (left axis). MODIS ET data and CRU precipitation data are presented in lighter colors, and modeled results are presented in lighter colors. Average monthly soil moisture values are also presented (right axis) using circle markers for each soil depth level: 10 cm (pink), 30 cm (red), 60 cm (orange), and 100 cm (yellow). The soil becomes saturated at the top level in November, and this corresponds with a marked increase in runoff and decrease in evapotranspiration in December. (right) Results of model runs IALU_C (C, darker colors) and IALUC_SMC (SMC, lighter colors). Again, average monthly evapotranspiration is presented in green, precipitation in blue, and runoff in purple. Runoff increases earlier in the growing season in IALU_SMC, where maximum soil moisture content and reference soil moisture content values were halved, decreasing evapotranspiration in August, September, and October. Results for subregions are presented in the supporting information.

results from the nested output are not improved compared to the 36 km grid cell output (Figures S7 and S8). ET in the nested output is similar to the 36 km output, with increases only in November and December. Precipitation is overestimated in December through March across both land cover types, and the source of this uncharacteristic overestimation warrants further exploration. Although the shape of the seasonal cycle of nested average monthly temperature more closely matches that of the observed, the mean monthly temperature is overestimated by 2–3° during the beginning of the rainy season and underestimated toward the end of the rainy season. It should be noted that the 12 km simulations used the same parameterization scheme as the 36 km simulations. Further exploration of parameterization schemes at the 12 km grid cell resolution might yield better results.

3.8. Determining the Sources of Model Error

Changing the cumulus scheme from Grell 3D to Kain-Fritsch (Model Runs IALU_C and IALU_A in Table 2, respectively) did not provide a justifiable fix for the temperature bias. Although the temperature bias generally decreased during the rainy season with the Kain-Fritsch cumulus scheme was used (IALU_A), the resulting change in modeled precipitation was overestimated by over 200% in some rainy season months (Figures 6 and S9). It may seem counterintuitive that both precipitation and temperature increased. However, as shown in Figure 6, average monthly incoming shortwave radiation also increased when the Kain-Fritsch scheme was used, which corresponds with the increasing temperature.

Neither the simulations using alternate soil moisture factor for stomatal resistance parameterizations (Table 2: IALU_rsf2 and IALU_rsf3) nor the simulations using different surface evaporation resistance options (Table 2: IALU_btr2 and IALU_btr3) affected ET rates (Figure S10). Furthermore, quadrupling the minimum stomatal resistance parameter of the agricultural land covers also did not affect ET: the average monthly stomatal resistance of both IALU_C and IALU_rsX4 are nearly the same (Figure S11). There may be no overall change because the vegetation parameter that was quadrupled in the static table simply represents the minimum stomatal resistance. Within the WRF model code, ET also depends on a land cover-specific parameter for optimum transpiration temperature, the vapor pressure deficit, a land cover specific parameter used in the radiation stress function, a land cover specific parameter used in the vapor pressure deficit function, surface temperature, and the amount of photosynthetically active radiation. Thus, the minimum stomatal resistance value seems to not play a large role in changing overall stomatal resistance.

Only the model run where soil field capacity and maximum soil water content were halved noticeably affected ET rates at the beginning of the growing season (Figure S10). As highlighted in Figures 4 and 5, ET is overestimated but precipitation is not, and ground evaporation—not transpiration or the evaporation of intercepted water—comprises a majority of the overestimated ET between September and December.

Runoff only responds strongly to increased precipitation after the soil has become saturated (Figure 7). By decreasing the field capacity of soil moisture, the ratio of water allocated to runoff instead of ET changes earlier in the growing season (Figures 7, S12, and S13). This change in maximum soil water storage also increased the temperature throughout the entire year, which decreased the cold bias during the rainy season, and created a warm bias during the dry season (Figure 6).

4. Concluding Remarks

The ability of farmers in rainfed agricultural breadbaskets, such as Brazilian Cerrado, to successfully cultivate crops is dependent on a long, stable rainy season. Yet extensive land clearing in this region could perturb the system enough to drastically affect precipitation and temperature during the rainy season. To understand the mechanistic changes in climatological seasonality of this dynamic region, a major first step is incorporating the best possible representations of the landscape into a regional climate model and assessing its ability to accurately simulate the climate of Brazil.

This work, the first to use WRF to run 10-year-long climatological simulations across Brazil, provides important insights. All simulations reasonably captured observed precipitation across the region. However, the IALU data set improved model performance across all variables, especially in the dry-to-wet-season transition. The precipitation and ET with IALU during the dry season and dry-to-wet season transition highlight the integral role that vegetative cover, specifically LAI phenology, plays in local land-atmosphere interactions, and in turn, regional climate. Correctly simulating the water and energy budget during these months is especially important, as moisture in the dry-to-wet season transition is crucial to a rainy-season onset occurring months before the southward shift of the Intertropical Convergence Zone (Wright et al., 2017).

There remains ample room for improvement and future research. All simulations struggled to accurately simulate climate during the rainy season. Evaporation and temperature are consistently biased during the rainy season, yet as highlighted in Figures 5 and 7, it seems that these biases are in large part, due to the way soil moisture is parameterized in WRF. As demonstrated by this analysis, and studies across the Great Plains (Massey et al., 2016; Pei et al., 2014), the Noah-MP model has difficulty simulating soil-moisture, which directly affects ET rates, and indirectly affects temperature. Although an alternate cumulus scheme improved temperature estimates, it also caused an overestimation of precipitation by more than 200% during some rainy season months. The reasons for the differences in spatial biases in ET across the region warrants further study. Using a nested grid to increase model resolution did not improve simulations in this region; however, using different cumulus, radiation, or surface-layer schemes within the nested domain may improve model results. Lastly, the dynamic vegetation model embedded within the Noah-MP land surface model did not accurately predict observed LAI phenology in the heavily modified agricultural areas of Brazil.

References

Aragão, L. E. O. C., Malhi, Y., Barbier, N., Lima, A., Shimabukuro, Y., Anderson, L., & Saatchi, S. (2008). Interactions between rainfall, deforestation and fires during recent years in the Brazilian Amazonia. *Philosophical Transactions of the Royal Society, B: Biological Sciences*, *363*(1498), 1779–1785. https://doi.org/10.1098/rstb.2007.0026

Arima, E. Y., Walker, R. T., Perz, S., & Souza, C. Jr. (2016). Explaining the fragmentation in the Brazilian Amazonia forest. *Journal of Land Use Science*, *11*(3), 257–277. https://doi.org/10.1080/1747423X.2015.1027797

Bagley, J. E., Desai, A. R., Harding, K. J., Snyder, P. K., & Foley, J. A. (2014). Drought and deforestation: Has land cover change influenced recent precipitation extremes in the Amazon? *Journal of Climate*, *27*(1), 345–361. https://doi.org/10.1175/JCLI-D-12-00369.1

Butt, N., de Oliveira, P. A., & Costa, M. H. (2011). Evidence that deforestation affects the onset of the rainy season in Rondonia, Brazil. *Journal of Geophysical Research*, *116*, D11120. https://doi.org/10.1029/2010JD015174

Cai, X., Yang, Z.-L., David, C. H., Niu, G.-Y., & Rodell, M. (2014). Hydrological evaluation of the Noah-MP land surface model for the Mississippi River Basin. *Journal of Geophysical Research: Atmospheres*, *119*, 23–38. https://doi.org/10.1002/2013JD020792

Challinor, A. J., Watson, J., Lobell, D. B., Howden, S. M., Smith, D. R., & Chhetri, N. (2014). A meta-analysis of crop yield under climate change and adaptation. *Nature Climate Change*, *4*(4), 287–291. https://doi.org/10.1038/nclimate2153, http://www.nature.com/nclimate/journal/v4/n4/abs/nclimate2153.html#supplementary-information

Coe, M. T., Brando, P. M., Deegan, L. A., Macedo, M. N., Neill, C., & Silvério, D. V. (2017). The forests of the Amazon and Cerrado moderate regional climate and are the key to the future. *Tropical Conservation Science*, *10*, 194008291772067. https://doi.org/10.1177/1940082917720671

Costa, M. H., Botta, A., & Cardille, J. A. (2003). Effects of large-scale changes in land cover on the discharge of the Tocantins River, Southeastern Amazonia. *Journal of Hydrology*, *283*(1–4), 206–217. https://doi.org/10.1016/S0022-1694(03)00267-1

Costa, M. H., & Pires, G. F. (2010). Effects of Amazon and Central Brazil deforestation scenarios on the duration of the dry season in the arc of deforestation. *International Journal of Climatology*, *30*(13), 1970–1979. https://doi.org/10.1002/joc.2048

Costa, M. H., Yanagi, S. N. M., Souza, P. J. O. P., Ribeiro, A., & Rocha, E. J. P. (2007). Climate change in Amazonia caused by soybean cropland expansion, as compared to caused by pastureland expansion. *Geophysical Research Letters*, *34*, L07706. https://doi.org/10.1029/2007GL029271

Da Rocha, R., Goncalves, F. L. T., & Segalin, B. (2015). Fog events and local atmospheric features simulated by regional climate model for the metropolitan area of Sao Paulo, Brazil. *Atmospheric Research*, *151*, 176–188. https://doi.org/10.1016/j.atmosres.2014.06.010

Dee, D. P., Uppala, S. M., Simmons, A. J., Berrisford, P., Poli, P., Kobayashi, S., et al. (2011). The ERA-Interim reanalysis: Configuration and performance of the data assimilation system. *Quarterly Journal of the Royal Meteorological Society*, *137*(656), 553–597. https://doi.org/10.1002/qj.828

Dubreuil, V., Debortoli, N., Funatsu, B., Nédélec, V., Durieux, L., Dubreuil, V., et al. (2012). Impact of land-cover change in the Southern Amazonia climate: A case study for the region of Alta Floresta, Mato Grosso, Brazil. *Environmental Monitoring and Assessment*, *184*(2), 877–891. https://doi.org/10.1007/s10661-011-2006-x

Friedl, M. a., McIver, D. K., Hodges, J. C. F., Zhang, X., Muchoney, D., Strahler, A. H., et al. (2002). Global land cover mapping from MODIS: Algorithms and early results. *Remote Sensing of Environment*, *83*(1-2), 287–302. https://doi.org/10.1016/S0034-4257(02)00078-0

Friedl, M. A., Sulla-Menashe, D., Tan, B., Schneider, A., Ramankutty, N., Sibley, A., & Huang, X. (2010). MODIS Collection 5 global land cover: Algorithm refinements and characterization of new datasets. *Remote Sensing of Environment*, *114*(1), 168–182. https://doi.org/10.1016/j.rse.2009.08.016

Fu, R., Yin, L., Li, W., Arias, P. A., Dickinson, R. E., Huang, L., et al. (2013). Increased dry-season length over southern Amazonia in recent decades and its implication for future climate projection. *Proceedings of the National Academy of Sciences of the United States of America*, *110*(45), 18,110–18,115. https://doi.org/10.1073/pnas.1302584110

Gao, L., Hao, L., & Chen, X. W. (2014). Evaluation of ERA-interim monthly temperature data over the Tibetan Plateau. *Journal of Mountain Science*, *11*(5), 1154–1168. https://doi.org/10.1007/s11629-014-3013-5

Georgescu, M., Lobell, D. B., Field, C. B., & Mahalov, A. (2013). Simulated hydroclimatic impacts of projected Brazilian sugarcane expansion. *Geophysical Research Letters*, *40*, 972–977. https://doi.org/10.1002/grl.50206

Harris, I., Jones, P. D., Osborn, T. J., & Lister, D. H. (2014). Updated high-resolution grids of monthly climatic observations - the CRU TS3.10 dataset. *International Journal of Climatology*, *34*(3), 623–642. https://doi.org/10.1002/joc.3711

Hayhoe, S. J., Neill, C., Porder, S., Mchorney, R., Lefebvre, P., Coe, M. T., et al. (2011). Conversion to soy on the Amazonian agricultural frontier increases streamflow without affecting stormflow dynamics. *Global Change Biology*, *17*(5), 1821–1833. https://doi.org/10.1111/j.1365-2486.2011.02392.x

Klink, C., & Machado, R. B. (2005). Conservation of the Brazilian Cerrado. *Conservation Biology*, *19*(3), 707–713. https://doi.org/10.1111/j.1523-1739.2005.00702.x

Lathuillière, M. J., Johnson, M. S., & Donner, S. D. (2012). Water use by terrestrial ecosystems: Temporal variability in rainforest and agricultural contributions to evapotranspiration in Mato Grosso, Brazil. *Environmental Research Letters*, *7*(2), 24024. https://doi.org/10.1088/1748-9326/7/2/024024

Lee, J. E., Lintner, B. R., & Neelin, J. D. (2012). Reduction of tropical land region precipitation variability via transpiration. *Geophysical Research Letters*, *39*, L19704. https://doi.org/10.1029/2012GL053417

Lee, S.-J., & Berbery, E. H. (2012). Land cover change effects on the climate of the La Plata Basin. *Journal of Hydrometerology*, *13*(1), 84–102. https://doi.org/10.1175/JHM-D-11-021.1

Legates, D. R., & McCabe, G. J. (1999). Evaluating the use of "goodness-of-fit" measures in hydrologic and hydroclimatic model validation. *Water Resources Research*, *35*, 233–241. https://doi.org/10.1029/1998WR900018

Levy, M., Cohn, A., Lopes, A. V., & Thompson, S. (2017). Addressing rainfall data selection uncertainty using connections between rainfall and streamflow. *Scientific Reports*, *7*(1), 219. https://doi.org/10.1038/s41598-017-00128-5

Loarie, S. R., Lobell, D. B., Asner, G. P., Mu, Q., & Field, C. B. (2011). Direct impacts on local climate of sugar-cane expansion in Brazil. *Nature Climate Change*, *1*(2), 105–109. https://doi.org/10.1038/nclimate1067

Malhado, A. C. M., Pires, G. F., & Costa, M. H. (2010). Cerrado conservation is essential to protect the Amazon rainforest. *Ambio*, *39*(8), 580–584. https://doi.org/10.1007/s13280-010-0084-6

Malhi, Y., & Wright, J. (2004). Spatial patterns and recent trends in the climate of tropical rainforest regions. *Philosophical Transactions of the Royal Society of London – Biology*, *359*(1443), 311–329. https://doi.org/10.1098/rstb.2003.1433

Massey, J. D., Steenburgh, W. J., Knievel, J. C., Cheng, W. Y. Y., Massey, J. D., Steenburgh, W. J., et al. (2016). Regional soil moisture biases and their influence on WRF model temperature forecasts over the Intermountain West. *Weather and Forecasting*, *31*(1), 197–216. https://doi.org/10.1175/WAF-D-15-0073.1

Mu, Q., Heinsch, F. A., Zhao, M., & Running, S. W. (2007). Development of a global evapotranspiration algorithm based on MODIS and global meteorology data. *Remote Sensing of Environment*, *111*(4), 519–536. https://doi.org/10.1016/j.rse.2007.04.015

Mu, Q., Zhao, M., & Running, S. W. (2011). Improvements to a MODIS global terrestrial evapotranspiration algorithm. *Remote Sensing of Environment*, *115*(8), 1781–1800. https://doi.org/10.1016/j.rse.2011.02.019

Nepstad, D. C., de Carvalho, & Vieira, S. (1994). The role of deep roots in the hydrological and carbon cycles of Amazonian forests and pastures. *Nature*, *372*, 666–669. https://doi.org/10.1038/372666a0

New, M., Hulme, M., & Jones, P. (1999). Representing twentieth-century space-time climate variability. Part 1: Development of a 1961–90 mean monthly terrestrial climatology. *Journal of Climate*, *12*(3), 829–856. https://doi.org/10.1175/1520-0442(1999)012

Niu, G.-Y., Yang, Z.-L., Mitchell, K. E., Chen, F., Ek, M. B., Barlage, M., et al. (2011). The community Noah land surface model with multiparameterization options (Noah-MP): 1. Model description and evaluation with local-scale measurements. *Journal of Geophysical Research*, *116*, D12109. https://doi.org/10.1029/2010JD015139

Oliveira, L. J. C., Costa, M. H., Soares-Filho, B. S., & Coe, M. T. (2013). Large-scale expansion of agriculture in Amazonia may be a no-win scenario. *Environmental Research Letters*, *8*, 24021. https://doi.org/10.1088/1748-9326/8/2/024021

Oliveira, P. T. S., Nearing, M. A., Moran, M. S., Goodrich, D. C., Wendland, E., & Gupta, H. V. (2014). Trends in water balance components across the Brazilian Cerrado. *Water Resources Research*, *50*, 7100–7114. https://doi.org/10.1002/2013WR015202

Panday, P. K., Coe, M. T., Macedo, M. N., Lefebvre, P., & Castanho, A. D. d. A. (2015). Deforestation offsets water balance changes due to climate variability in the Xingu River in eastern Amazonia. *Journal of Hydrology*, *523*, 822–829. https://doi.org/10.1016/j.jhydrol.2015.02.018

Pei, L., Moore, N., Zhong, S., Luo, L., Hyndman, D. W., Heilman, W. E., et al. (2014). WRF model sensitivity to land surface model and cumulus parameterization under short-term climate extremes over the southern Great Plains of the United States. *Journal of Climate*, *27*(20), 7703–7724. https://doi.org/10.1175/JCLI-D-14-00015.1

Ruhoff, A. L., Paz, A. R., Aragao, L. E. O. C., Mu, Q., Malhi, Y., Collischonn, W., et al. (2013). Assessment of the MODIS global evapotranspiration algorithm using eddy covariance measurements and hydrological modelling in the Rio Grand basin. *Hydrological Sciences Journal*, *58*(8), 1658–1676. https://doi.org/10.1080/02626667.2013.837578

Ruiz, J. J., Saulo, C., Nogués-Paegle, J., Ruiz, J. J., Saulo, C., & Nogués-Paegle, J. (2010). WRF model sensitivity to choice of parameterization over South America: Validation against surface variables. *Monthly Weather Review*, *138*(8), 3342–3355. https://doi.org/10.1175/2010MWR3358.1

Ruiz-Arias, J. A., Arbizu-Barrena, C., Santos-Alamillos, F. J., Tovar-Pescador, J., & Pozo-Vázquez, D. (2016). Assessing the surface solar radiation budget in the WRF model: A spatiotemporal analysis of the bias and its causes. *Monthly Weather Review*, *144*(2), 703–711. https://doi.org/10.1175/MWR-D-15-0262.1

Sakaguchi, K., & Zeng, X. (2009). Effects of soil wetness, plant litter, and under-canopy atmopsheric stability on ground evaporation in the Community Land Model (CLM3.5). *Journal of Geophysical Reviews - Atmospheres*, *114*, D01107. https://doi.org/10.1029/2008JD010834

Sano, E. E., Rosa, R., Brito, J. L. S., & Ferreira, L. G. (2010). Land cover mapping of the tropical savanna region in Brazil. *Environmental Monitoring and Assessment*, *166*(1-4), 113–124. https://doi.org/10.1007/s10661-009-0988-4

Sellers, P. J., Heiser, M. D., & Hall, F. G. (1992) Relations between surface conductance and spectral vegetation indices at intermediate (100 m^2 to 15 km^2) length scales. *Journal of Geophysical Research*, *97*, 19,033–19,059. https://doi.org/10.1029/92JD01096

Silvério, D. V., Brando, P. M., Macedo, M. N., Beck, P. S. A., Bustamante, M., & Coe, M. T. (2015). Agricultural expansion dominates climate changes in southeastern Amazonia: The overlooked non-GHG forcing. *Environmental Research Letters*, *10*(10), 104015. https://doi.org/10.1088/1748-9326/10/10/104015

Simoes, A. J. G., & Hidalgo, C. A. (2011). The Economic Complexity Observatory: An analytical tool for understanding the dynamics of economic development. Workshops at the Twenty-Fifth AAAI Conference on Artificial Intelligence.

Skamarock, W. C., Klemp, J. B., Dudhia, J., Gill, D. O., Barker, D. M., Duda, M. G., et al. (2008). *A description of the Advanced Research WRF version 3. (NCAR/TN-475+STR)*. Boulder, CO: National Center for Atmospheric Research.

Spangler, K. R., Lynch, A. H., Spera, S. A., Spangler, K. R., Lynch, A. H., & Spera, S. A. (2017). Precipitation drivers of cropping frequency in the Brazilian Cerrado: Evidence and implications for decision-making. *Weather, Climate, and Society*, *9*(2), 201–213. https://doi.org/10.1175/WCAS-D-16-0024.1

Spera, S. A., Galford, G. L., Coe, M. T., Macedo, M. N., & Mustard, J. F. (2016). Land-use change affects water recycling in Brazil's last agricultural frontier. *Global Change Biology* https://doi.org/10.1111/gcb.13298, *22*(10), 3405–3413.

The World Bank (2017). World Bank Open Data, Table: Agricultural irrigated land (% of total agricultural land). Data from the Food and Agricultural Organization. Retrieved from https://data.worldbank.org/indicator/AG.LND.IRIG.AG.ZS?locations=BR

Vendemiatti, A., & Berk, C. (2016). *Brazil Agricultural Economic Fact Sheet, Global Agricultural Information Network Report. (BR15009)*. Sao Paulo: USDA Foreign Agricultural Service.

Wang, J., Chagnon, F. J. F., Williams, E. R., Betts, A. K., Renno, N. O., Machado, L. A. T., et al. (2009). Impact of deforestation in the Amazon basin on cloud climatology. *Proceedings of the National Academy of Sciences of the United States of America*, *106*(10), 3670–3674. https://doi.org/10.1073/pnas.0810156106

Wright, J. S., Fu, R., Worden, J. R., Chakraborty, S., Clinton, N. E., Risi, C., et al. (2017). Rainforest-initiated wet season onset over the southern Amazon. *Proceedings of the National Academy of Sciences*, *114*(32), 8481–8486. https://doi.org/10.1073/pnas.1621516114

Yang, Z.-L., Niu, G.-Y., Mitchell, K. E., Chen, F., Ek, M. B., Barlage, M., et al. (2011). The community Noah land surface model with multiparameterization options (Noah-MP): 2. Evaluation over global river basins. *Journal of Geophysical Research*, *116*, D12110. https://doi.org/10.1029/2010JD015140